Crystalline adducts of the Lawsone molecule (2-hydroxy-1,4-naphthaquinone): optical properties and computational modelling

Journal Name

Dynamic Article Links ►

Cite this: DOI: 10.1039/c0xx00000x

www.rsc.org/xxxxxx

ARTICLE TYPE

Crystalline Adducts of Lawsone molecule (2-hydroxy-1,4-naphthaquinone): optical properties and computational modelling

Anuradha Pallipurath,[a] and Jonthan M. Skelton, *[c] Amit Delori,[b] Connor Duffy,[a] Andrea Erxleben,[a] and William Jones[d]

Received (in XXX, XXX) Xth XXXXXXXXX 20XX, Accepted Xth XXXXXXXXX 20XX

DOI: 10.1039/b000000x

Four new heterodimers of the Lawsone molecule (2-hydroxy-1,4-naphthaquinone) with 4,4'-bipyridine, 4-(2-pyridine-4-ethyl)pyridine, 1,3-di(4-pyridyl)propane and 2-hydroxy pyridine are reported. Cocrystalisation leads to colour shifts from orange in pure Lawsone to yellow and red, which are characterised by UV/visible spectroscopy. Complementary quantum-chemical calculations are used to study the energetics of the cocrystal formation, and to gain insight into the origin of the observed colour changes.

The naturally-occurring compound Lawsone (2-hydroxy-1,4-naphthoquinone) has been in use for the past 5000 years for utilities ranging from traditional tattoo ink (henna) to medicinal remedies. Since it is an abundant naturally-occurring dye, it is used as an artificial tanning agent and a hair colourant. Its good UV-absorbing properties makes it a good anti-tanning agent.[1, 2] Lawsone has also been identified as having anti-fungal,[3] anti-corrosion[4] and even anti-cancer properties,[5] and has also been intercalated into Zn hydroxides to act as a drug-delivery system.[6] It reacts with primary amino acids to form photoluminescent products, which can be used to detect fingerprints.[7]

Due to its C=O and O-H functional groups, Lawsone readily forms Michael-addition products and Mannich bases,[8] some of which have antimalarial properties.[9, 10] These functional groups also make the molecule an ideal candidate for forming polymorphs and cocrystals with amines, though supramolecular self-organisation mediated by H-bonding interactions. In 2005, Todkary *et al*. reported the existence of different polymorphic forms of Lawsone, formed through solvent interactions.[11] They predicted the formation of a molecular-tape-like structure in the presence of protic polar solvents, and a herringbone-like structure in the presence of aprotic solvents such as acetone. They also observed intrinsic radical formation in both polymorphs, arising from electron-density percolation through intermolecular hydrogen bonds, using EPR spectroscopy.

In contrast, the most recently-reported cocrystals of Lawsone, with Tris(hydroxymethyl)aminomethane[12] were found to be EPR inactive. In addition to π-stacking interactions between Lawsone molecules and H-bonding interactions between Lawsone and Tris(hydroxymethyl)aminomethane along the crystallographic *a* axis, a proton transfer from Lawsone to the coformer was also observed in the cocrystal.

We have previously carried out similar co-crystallisation through ball milling to improve solubility, and, modify the colour of fluorescein pigment[13]. We have also shown a multi-colour fluorescence emission, along with two photon luminescence in stilbene-like compounds[14] achieved though supramolecular chemistry, without any synthetic chemical modification.

In this paper, we report crystalline adducts of Lawsone with four different amines, *viz*. 4,4'-bipyridine, 4-(2-pyridine-4-ethyl)pyridine, 1,3-di(4-pyridyl)propane and 2-hydroxy pyridine. All four cocrystals exhibit changes in colour with respect to neat Lawsone, and we observe a proton transfer from Lawsone to the coformer in the adduct with 4-(2-pyridine-4-ethyl) pyridine and a tautomerisation in case of the adduct with 2-hydroxyl pyridine. We also carry out complementary density-functional theory calculations to model the energetics of the cocrystal formation, and to investigate the origin of the colour changes in terms of the electronic structure.

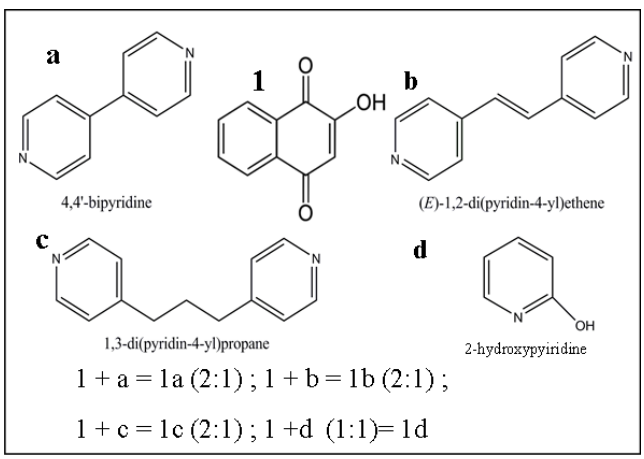

Chart 1 Molecular structures of Lawsone (**1**), 4,4'-bipyridine (**a**), 4-(2-pyridine-4-ethyl)pyridine (**b**), 1,3-di(4-pyridyl)propane (**c**) and 2-hydroxy pyridine (**d**), together with reaction equations detailing the stoichiometry of cocrystal formation.

Cocrystallization reactions between Lawsone (**1**) and the coformers 4,4'-bipyridine, 4-(2-pyridine-4-ethyl)pyridine, 1,3-di(4-pyridyl)propane and 2-hydroxy pyridine (**a-d**) were carried out to obtain the adducts **1a-1d** (Chart 1). The solid-state structures of the adducts were obtained from single-crystal X-ray diffraction (XRD), and the crystals were further characterised by

microscopy, thermal analysis, near-infrared (NIR) spectroscopy and UV/visible reflectance. The synthesis and characterisation procedures are described in detail in the Methods section.

Figure 1 shows the crystal packing in **1a**-**1d**; these are also available from the CCDC under the codes **[X]**, **[Y]**, **[Z]** and **[W** In **1a**-**1c**, the coformers act as spacers, joining two molecules of **1** and forming discrete 3-membered supramolecular assemblies (see Figure 1a, 1c and 1e). In contrast, coformer **d** forms a dimer of its tautomer, and the $\mathbf{d}_2$ tautomeric unit plays an equivalent role to **a**-**c** in **1d**. This gives rise to different Lawsone:coformer ratios in the cocrystals, with 2:1 and 1:1 stoichiometries in **1a**-**1c** and **1d**, respectively.

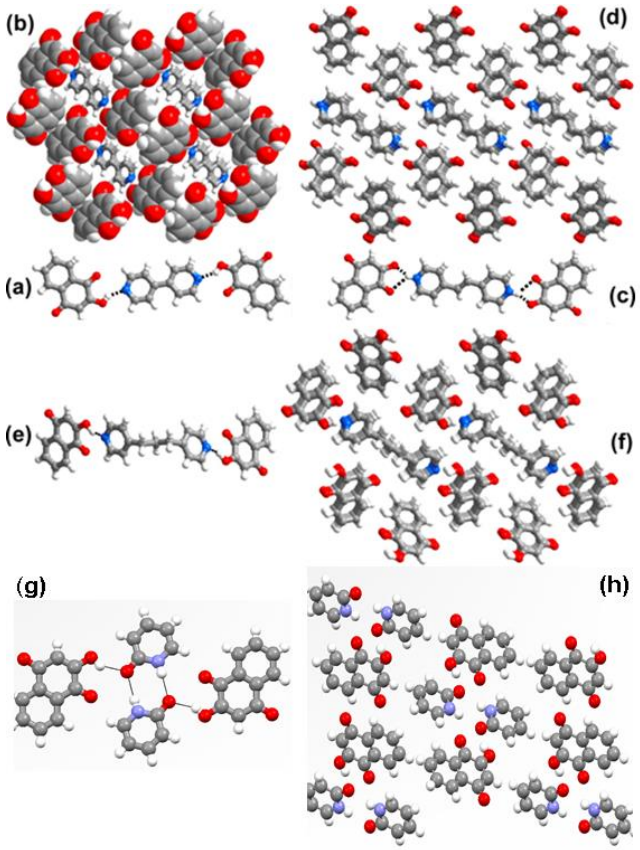

Fig. 1 Crystal packing in the cocrystals of **1a** (a, b), **1b** (c, d), **1c** (e, f) and **1d** (g, h).

1a, 1b and **1d** crystallise into the monoclinic space group $P2_1/n$. In **1a** and **1b** structures, the heterodimers adopt linear geometries, but while the two Lawsone molecules and the coformer are almost coplanar in **1a**, the former are significantly tilted out of the plane in **1b**. Interestingly, despite coformer **b** in principle being fully conjugated, it exhibits some distortion from a perfect planar geometry in the crystal structure. Interestingly, the crystal structure of **1b** shows a proton transfer from Lawsone to the coformer, which is not observed in the structure of **1a**. From packing diagrams, it can be seen that in 3 dimensions the coformer molecules are sandwiched between tapes of **1** (see Figures 1b, 1d and 1f); in **1a**, the molecular tapes of **1** are arranged in such a way as to lead to the formation of a host-guest complex. Due to the propyl group in coformer **c**, **1c** adopts a herring-bone geometry, and crystallises in the orthorhombic space group *Fdd*2.

In **1a**, **1c** and **1d**, **1** interacts with the coformers through neutral O-H···N hydrogen bonds, whereas in **1b** cations of **b** interact with anions of **1** by both $N\text{-}H^{+}\cdots O^{-}$ and $N\text{-}H^{+}\cdots O$ hydrogen bonds. This is supported by the NIR spectra (see supporting information), in which O-H combination bands are seen in **1a** and **1c**, but not in **1b**, in **1d** the combination bands observed are of amide III groups[15]. The case of **1d** is quite peculiar, as the conformer **d** underwent tautomerisation to give 2-pyridone, as noted in the literature [16]. Initially, the formation of a zwitter ion was suspected, but the C-O bond distance of 1.26Å, suggested that the bond was a double bond, and the melting point determined by DSC was also much lower, compared to that of salt **1b**. A similar bond length was observed by other works in the literature[17]. A six membered ring is formed through inter molecular hydrogen bonding between the two 2-pyridone. The carbonyl oxygen from the 2-pyridone also forms inter molecular hydrogen bonds with the hydroxyl group from naphthoquinone. This hydrogen bond is the shortest at 1.93Å. Such homodimer formation has been observed in cocrystals of carbamezipine, where the homosynthon formed by the amide hydrogen bonding, forms 1D H-bonds with the co-former[18]. Henceforth **d** and **1d** will refer to 2-pyridone and its adduct with lawsone respectively. Conformer **b** and **d**, are known to undergo photodimerisation reactions[17, 19]. In **1b** the distances between the C=C in **b**, in adjacent layers is 3.816 Å and, in **1d** the distances between **d** in consecutive layers is 5.153 Å. These distances are slightly longer than the ideal condition for photodimerisation (1.727 (4)–3.324 (4) Å). Hence, we do not except to see any photodimerisation[17].

To study the crystal morphologies, we recorded bright-field microscope images of the four cocrystals (Figure 2). **1a** formed blocky crystals, while **1b** formed bladed crystals. **1c** and **1d** formed needle-like crystals. The figure 2d of the cocrystal **1d** is from a mounted crystal as a polarising microscope was not available at the time of preparation.

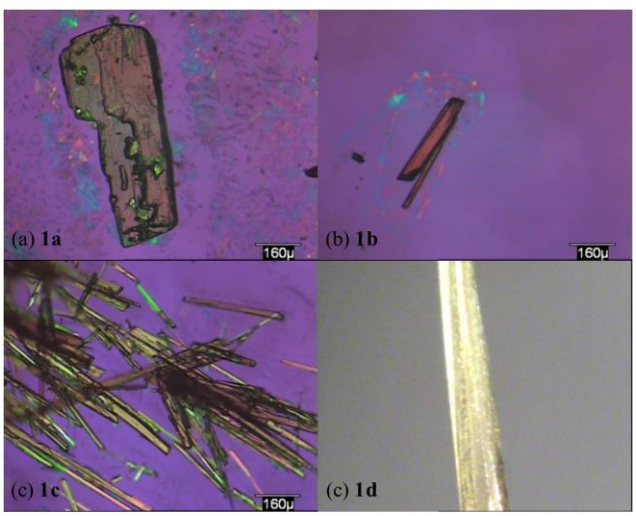

Fig. 2 Bright-field microscope images of the cocrystals of Lawsone with 4,4'-bipyridine (**1a**, a), 4-(2-pyridine-4-ethyl)pyridine (**1b**, b) and 1,3-di(4-pyridyl)propane (**1c**, c), taken under polarised light, and an image of a single crystal of the 2-hydroxypyridine cocrystal (**1d**, d) mounted on a diffractometer pin.

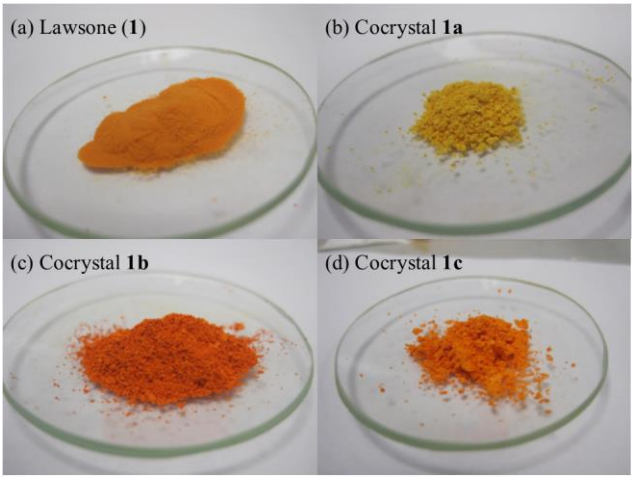

Fig. 3 Photographs of Lawsone (**1**; a**)** and the cocrystals synthesised using 4,4'-bipyridine (**1a**; b), 4-(2-pyridine-4-ethyl)pyridine (**1b**; c) and 1,3-di(4-pyridyl)propane (**1c**; d), illustrating the observed colour changes.

Finally, we further characterised cocrystals **1a-1d** by differential-scanning calorimetry (DSC; see supporting information). The DSC traces show **1b** to have the highest melting point of 210.14°C, compared to 183.96 and 155.80 °C for **1a** and **1c**, respectively. This is naturally accounted for by the stronger ionic hydrogen bonds in **1b**. The melting point of **1d** was observed to be 147.9°C.

Cocrystallisation also led to clear differences in colour with respect to neat Lawsone (Fig. 3). Cocrystalisation with **a** and **d** gives rise to a hypsochromic shift in colour, while in contrast **1c** and **1b** both undergo bathochromic colour shifts (see supporting info for image of **1d**). From the UV-visible reflectance spectra (Fig 4 a), differences in the colour of neat Lawsone and **1a-1d** are again clearly evident. We also recorded solution spectra in a 2:1 mixture of acetonitrile and methanol (Fig. 4b), and these show small sholder like features in the visible region in the case of **1b** and **1c**, but these were weak in comparison to the absorption seen in the UV. **1a** and **1d** show no prominent features in the visible region.

To better understand the energetics of the cocrystal formation and the origin of the colour change, we carried out complementary theoretical modelling within the density-functional theory (DFT) formalism (see Methods).

As a starting point, we first fully relaxed the crystal structures of **1a-1d** with the PBEsol functional,[20] optimising both the positions of the ions and the unit-cell shape/volume. We also relaxed gas-phase models of Lawsone and the four coformers **a-d**, the $\mathbf{d}_2$ dimer, and the heterodimers **1a-1d**, made by extracting the relevant species from the collected crystal structures. Finally, to obtain more accurate energetics and electronic structures, and to calculate the optical-absorption spectra of the solid-state species, we performed single-point calculations on the PBEsol-optimised models using the PBE0 hybrid functional.[21]

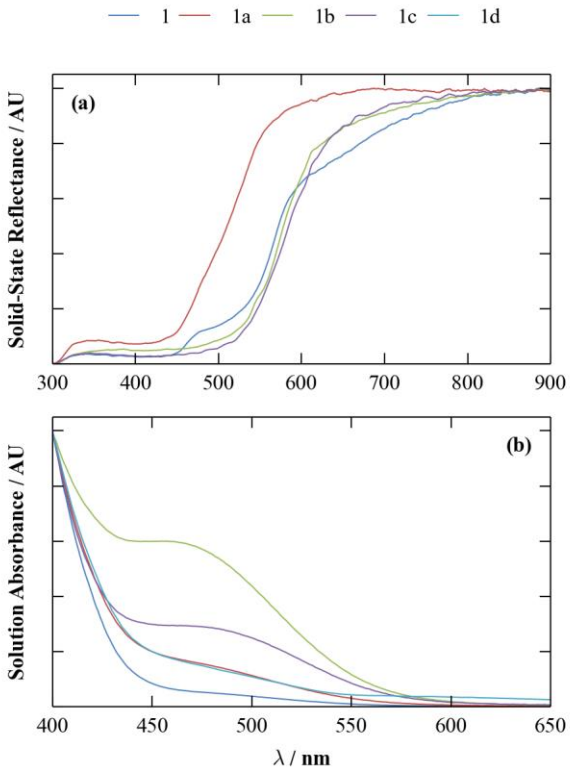

Fig. 4 Optical properties of Lawsone (**1**) and its cocrystals with 4,4'-bipyridine (**1a**), 4-(2-pyridine-4-ethyl)pyridine (**1b**), 1,3-di(4-pyridyl)propane (**1c**) and 2-hydroxy pyridine (**1d**). The two plots show the normalised solid-state reflectance spectra of **1** and **1a-1c** (a), and the solution absorbance spectra of **1** and **1a-1d** (b), recorded in the wavelength range 300-900 and 400-650 nm, respectively. To better identify the position of the transition edges in the reflectance spectra, the first derivatives were calculated by numerical differentiation (see supporting information).

The calculated unit-cell parameters are compared to the experimental structures in the supporting information. We found that PBEsol gave a fairly good reproduction of the structures, with a tendency to overestimate the cell volume, but with <5 % variation in most parameters. The discrepancy in the cell volume in **1a-1c** was found to be mostly due to a consistent overestimate of the length of the short lattice vectors, which we attributed to PBEsol not being able to describe fully the attractive part of the dispersive interaction between molecules along the stacking direction. In support of this, the single-point PBE0 calculations predicted negative cell pressures, implying that a better description of non-local electron correlation would indeed lead to a reduction in the cell volume.

After optimising the heterodimers in the gas phase, we found they generally retained a structure similar to that in the solid form, with the exception of the proton transfer in **1b**. In both the experimental and the PBEsol-optimised crystal structures, the proton lies between the coformer N and the Lawsone O. After optimisation of the gas-phase adduct, however, it appears to be mainly associated with the latter group as is the case in the other cocrystals. Images of the optimised gas-phase adduct and crystal structure of **1b** are given in the supporting information for comparison. This observation suggests that the proton transfer is

a consequence of the crystal packing, and the resultant intermolecular interactions, in the solid form.

To investigate the energetics of the cocrystal formation, we calculated the formation energies of the gas-phase heterodimers and crystals of **1a**-**1d** (Table 1). To first approximation, the formation energies of the gas-phase heterodimers correspond to the energy of the H-bonding interactions, while the (per-adduct) differences in E_F between the gas-phase and crystal structures gives an indication of the strength of the interactions between heterodimers in the solid state.

	[kJ mol^{-1} Adduct^{-1}]			
	PBEsol		PBE0@PBEsol	
Species	E_F	ΔE	E_F	ΔE
d homodimer	-104.17	-	-78.39	-
1a heterodimer	-87.19	-	-46.74	-
1b heterodimer	-89.25	-	-47.61	-
1c heterodimer	-92.28	-	-50.71	-
1d heterodimer	-187.18	-	-130.16	-
Crystal **1a**	-161.35	-74.15	-96.87	-50.13
Crystal **1b**	-185.46	-96.20	-110.47	-62.87
Crystal **1c**	-176.64	-84.36	-	-
Crystal **1d**	-234.21	-47.03	-154.16	-24.00

Table 1 Calculated formation energies of the gas-phase heterodimers and corresponding crystal structures of **1a**-**1d**, plus the gas-phase homodimer of **d**. Two sets of energies are given; the first were obtained from models fully relaxed with the PBEsol functional, while the second were obtained from single-point calculations on these models with the PBE0 hybrid functional (denoted "PBE0@PBEsol"). In each set, the left-hand column gives the formation energies, while the right-hand one gives the differences between the crystals and gas-phase heterodimers. We note that PBE0@PBEsol values for the crystal of **1c** are missing, as the size of the unit cell made it impractical to perform these calculations at the same level of accuracy as for the others.

For **1a**-**1c**, the PBEsol and PBE0 calculations predict the energy of each Lawsone-coformer H bond to be on the order of 45 and 25 kJ mol^{-1}, respectively, increasing in the order **c** > **b** > **a**. In adduct **1d**, there are two types of H bond, *viz.* those between the two 2-hydroxy pyridine molecules, and those between the coformer and Lawsone; for the present discussion, we estimate the two contributions from the difference in the formation energies of the $\mathbf{d}_2$ dimer and adduct **1d** in the gas phase. The **d**-**d** interaction is stronger than the bond between the dimer and Lawsone at ~50/40, and 40/25 kJ mol^{-1} per bond with PBEsol and PBE0, respectively, which may be due to a stronger electrostatic component due the proton transfer. Interestingly, PBEsol predicts the bond between the coformer **d** and Lawsone to be the weaker of the four, whereas PBE0 predicts it to be the strongest. Nonetheless, the range in the calculated bond strengths between Lawsone and **a**-**c** and $\mathbf{d}_2$ is fairly small at <5 (PBEsol) and < 2.5 (PBE0) kJ mol^{-1}.

For heterodimers 1**a**-1**c**, the per-adduct energy gain due to intermolecular interactions in the crystal is of a similar magnitude to the H-bonding in the gas phase, being around 85 and 55 kJ mol^{-1} with PBEsol and PBE0, respectively, for 1**a**-1**c**. **1d** behaves a little differently in this respect, with the energy difference between the gas phase and solid forms being around half that between the gas-phase adduct and the isolated Lawsone and $\mathbf{d}_2$ species. The reasons for this are not clear, but this analysis nonetheless provides some interesting insight into the relative energetic stabilisation provided by H-bonding and π-stacking interactions.

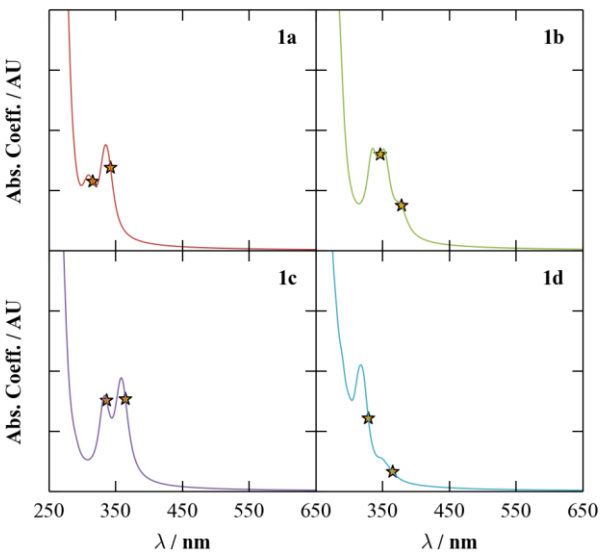

Fig. 5 Simulated absorption spectra of crystals **1a**-**1d** in the range of 250-650 nm, obtained at the PBE0 hybrid level of theory on the PBEsol-relaxed structures. The yellow stars mark the positions of the direct band gaps at the two ***k***-points modelled in each structure.

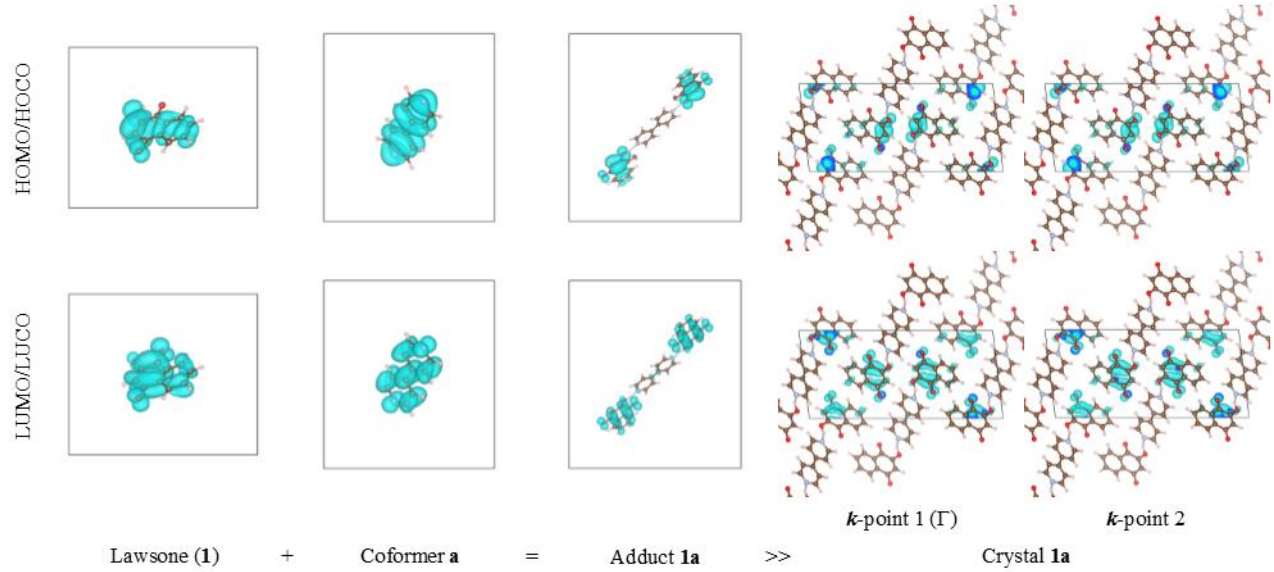

Fig. 6 Orbital-density plots illustrating the relationship between the frontier orbitals of Lawsone (**1**), coformer **a**, the gas-phase **1a**, and the corresponding solid form. For the latter, the frontier orbitals at both ***k***-points used to model the electronic structure are shown (see discussion in text).

Next, we used the PBE0 calculations to investigate the electronic structure of the molecules, and crystals. Fig. 6 shows the calculated absorption spectra of crystals **1a**-**1d**. The four spectra are qualitatively similar in form, with a handful of features between 300-400 nm, a steep rise below ~250 nm, and a smooth tail off above 400 nm. The spectra in Fig. 4 (b) were recorded only to 400 nm, so it is difficult to assess the correspondence between these and the calculated absorption profiles. However, most appear to display the same long tails, and a the small shoulder at ~375 nm in the calculated spectrum of **1b** might be equated to the broad absorption at ~475 nm in the corresponding spectrum in Fig. 4. If this is the case, it implies that the calculated spectra are blue shifted by around 100 nm with respect to the experimentally-recorded ones, which can be attributed to the approximations in the time-dependent DFT (TD-DFT) method employed in these simulations.[22]

A feature highlighted in Fig. 5 is that in all four crystals the main absorption features match up quite well with the energy gap between the highest-occupied and lowest-unoccupied crystal orbitals (HOCOs/LUCOs) at the two ***k***-points used to model the electronic structure. This implies that an analysis of the frontier orbitals and energy gaps in the crystals, and component species may provide some insight into the origin of the observed colour changes on cocrystal formation. Table 2 compares the calculated gaps in Lawsone (**1**), coformers **a**-**d**, the $\mathbf{d}_2$ dimer, and s **1a**-**1d** and their crystalline forms.

Lawsone has a smaller energy gap than any of the four coformers, being >1 eV narrower than the gaps of coformers **a** and **c**, ~1 eV narrower than the energy gaps of **d** and its dimer, which are fairly similar, and ~400 meV narrower than the HOMO-LUMO gap of **b**. The gaps of **a**, **b** and **c** fall into the order **c** > **a** > **b**, which is consistent with the degree of conjugation in these molecules. Taking the gas-phase energy gap of Lawsone as a reference, the gaps of the s are consistently smaller by 200-400 meV. In all four of the solid-state structures, convergence testing found that two ***k***-points were required along the short lattice vector, corresponding to the π-stacking direction, to describe the electronic wavefunctions, which implies that there are significant interactions between the localised orbitals of adjacent s in the electronic bands of the crystal. The HOCO-LUCO gaps at these two ***k***-points are generally narrowed by 200-500 meV with respect to the gas-phase s, with the exception being the gaps of **1a** and **1d** at the zone centre (Γ), which show relatively small increases of 20 and 40 meV, respectively.

Species	$E_{g,1}$ / eV (nm)	Δ1 / meV	$E_{g,2}$ / eV (nm)	Δ1 / meV
Lawsone (**1**)	4.121 (301)	-	-	-
Coformer **a**	5.544 (224)	-	-	-
Coformer **b**	4.508 (275)	-	-	-
Coformer **c**	6.357 (195)	-	-	-
Coformer **d**	5.105 (243)	-	-	-
(Coformer **d**)$_2$	5.141 (241)	-	-	-
1a heterodimer	3.907 (317)	-214	-	-
1b heterodimer	3.767 (329)	-355	-	-
1c heterodimer	3.887 (319)	-234	-	-
1d heterodimer	3.732 (332)	-389	-	-
Crystal **1a**	3.927 (316)	-195	3.622 (342)	-500
Crystal **1b**	3.579 (346)	-543	3.277 (378)	-844
Crystal **1c**	3.685 (336)	-436	3.400 (365)	-722
Crystal **1d**	3.774 (329)	-348	3.396 (365)	-726

Table 2 Calculated energy gaps (E_g) of Lawsone (**1**), coformers **a**-**d** and the homodimer of **d**, the gas-phase s **1a**-**1d**, and the corresponding crystal structures. For the latter, two gaps are given, one for each of the *k*-points used to model the wavefunctions. For the s and crystals, the difference between the energy gaps and that of the Lawsone molecule are shown in the adjacent columns.

By analysing orbital-density plots obtained from the PBE0 calculations, we found that the form of the HOMOs and LUMOs of the s could be qualitatively well understood in terms of the frontier orbitals of the component species. In s **1a** and **1c**, the HOMO and LUMO are both linear combinations of the corresponding Lawsone orbitals. In **1b**, the HOMO is on the Lawsone molecules, whereas the LUMO resides on the

conformer, and the reverse occurs in **1d**. There is little evidence of electronic delocalisation between the Lawsone and coformer molecules in the s, nor, by extension, between the Lawsone molecules across the bridging coformers. In all four systems, the HOMO and LUMOs of the s match up very well with the HOCOs and LUCOs of the crystals, respectively, with the orbital densities at both ***k***-points being visually near identical. An example orbital-density analysis for **1a** is illustrated in Fig. 6, and similar analyses for **1b**-**1d** may be found in the supporting information.

Given the similarity between the frontier orbitals of the s in the gas phase and solid state, we can infer that the narrower energy gap in the latter, noted above, is due to a significant extent to the intermolecular interactions. In **1a** and **1c**, the HOMO and LUMO in the s are both on Lawsone, so it is reasonable to suggest that the narrowing of the gap is due to the frontier orbitals on Lawsone being perturbed by the H-bonding interaction with the coformer. For **1b** and **1d**, the coformer provides a lower-energy LUMO and higher-energy HOMO, respectively, and so the narrowing of the gap with respect to neat Lawsone cannot be attributed solely to the H-bonding interaction in this way. It is worth noting, however, that this may account for why the gap of these s undergoes a larger shift with respect to Lawsone than those of **1a** and **1c**.

To explore this further, and to investigate how reliably the frontier orbitals of the isolated component molecules might be used to predict those of the s (and hence the crystals), we constructed orbital-alignment diagrams matching up the HOMOs and LUMOs of Lawsone and coformers with four highest-occupied and lowest-unoccupied orbitals of the s (Fig. 7). The reason for our considering four orbitals is that the molecular orbitals from the two Lawsone molecules in the s generally formed (near-)degenerate pairs, corresponding to in-phase and antiphase combinations which, when performing the alignment, the orbital energies were adjusted to the electrostatic potential in the vacuum region of the cells.[23] We note that this procedure cannot be applied to bulk materials (at least not those without a sufficiently large internal pore[23]), and so we were unable to perform a similar comparison between the heterodimers and the crystals.

The analysis in Fig. 7 shows that, in general, the frontier orbitals of Lawsone and the coformer are significantly perturbed on adduct formation. The H-bonding appears to cause the Lawsone orbitals to shift to higher energies, while those of the coformer are lowered with respect to the isolated species.

In the case of heterodimers **1a** and **1c**, the where the HOMO and LUMO of the adduct are both Lawsone-based, the HOMO of the coformer is below that of Lawsone, and thus the stabilisation in the adduct serves to push it further below the Lawsone orbitals. Similarly, although the coformer LUMO is lowered in energy, this is insufficient to bring it below the Lawsone-based LUMO observed in these heterodimers, although the alignment diagram for **1a** shows that they are close in energy. In these two heterodimers, the primary origin of the colour shift in the gas-phase adduct can be ascribed to a slight difference in the relative destabilisation of the HOMO and LUMO, which serves to narrow the energy gap.

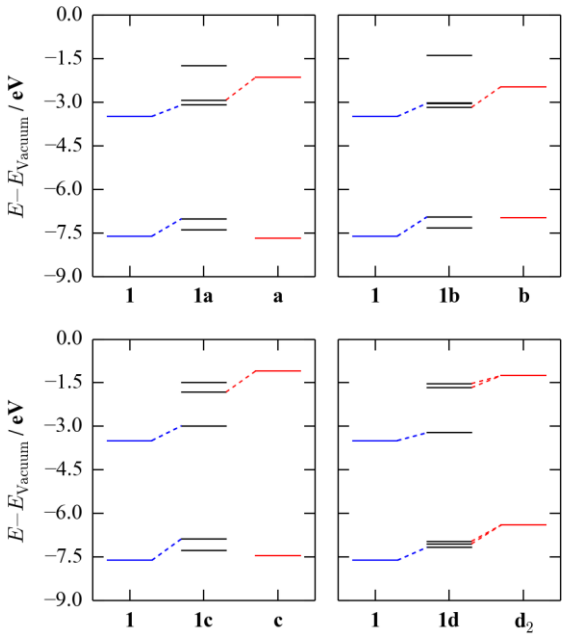

Fig. 7 Orbital-alignment diagrams for heterodimers **1a**-**1d**. Each Plot shows the position of the HOMO and LUMO of Lawsone (blue) and the coformer (red) with respect to the four highest-occupied and lowest-unoccupied orbitals of the adduct (black). Dashed lines are drawn between orbitals in the component species which are related to those in the adduct. All energies are expressed relative to the vacuum level. For adduct **1d**, the $\mathbf{d}_2$ dimer, rather than the isolated molecule, was used as the coformer in the alignment.

Considering the other two heterodimers, in **1b** the destabilisation of the Lawsone-based LUMO and stabilisation of the coformer orbitals is sufficient to push the LUMO in the adduct onto the coformer. In **1d**, the HOMO on the coformer is above that of Lawsone, and in this case the rearrangement of the orbital energies is insufficient to swap the order, leading to a coformer-based HOMO in this adduct, although as in **1a** the two HOMOs are close in energy.

The energy shifts make it somewhat difficult to predict *a priori* the relationship between the frontier orbitals in Lawsone and the coformers and those in the adduct. However, given that the direction of the shift appears to be a consistent trend, we can extract two general observations: (1) if the HOMO on the coformer is below or similar in energy to that on Lawsone, the Lawsone orbital will likely become the HOMO on the adduct, and (2) if the LUMOs on the two components are similar in energy, or if the orbital on the coformer is below the Lawsone LUMO, the LUMO in the adduct will likely be Lawsone-based. Using these principles, it may be possible to assess qualitatively how other potential coformers may shift the colour of neat Lawsone using relatively cheap gas-phase calculations.

Conclusions

Four cocrystals of the Lawsone molecule with bipyridine, ethylenebipyridine, propylenebipyridine and 2-hydroxypyridine were synthesised and characterised using single-crystal X-ray diffraction, thermal analysis, UV-visible and IR spectroscopy. Three of the coformers yielded crystals based around three-

membered complexes consisting of one conformer and two Lawsone molecules, while the fourth gave a 1:1 complex with a similar structure based around a H-bonded dimer of the coformer. Whereas Lawsone and the coformer in the bipyridine and propylenebipyridine cocrystals interact through neutral H bonds, the ethylenebipyridine system shows a solid-state proton transfer, which is also clearly evident from its IR spectrum. The 2-hydroxy pyridine system also displays a proton transfer, but between the conformer molecules, which exist as zwitterions in the adduct. The cocrystals were all found to exhibit visible shifts in colour with respect to neat Lawsone.

The hierarchy of interactions in the cocrystal formation, *viz.* H-bonding between Lawsone and the coformers and intermolecular π-stacking in the solid state, allowed us to use computational modelling to study the contributions of the various effects to the energetics and colour shift. Both interactions lead to roughly equal energetic gains on cocrystal formation, and the typical H-bond strength between Lawsone and one of the coformers was calculated to be on the order of 25 kJ mol^{-1} at the hybrid level of theory. It was also noted that the proton transfer in **1b** was not observed in the gas-phase adduct, suggesting that this is a product of the intermolecular interactions in the solid state. The long-wavelength absorption features in the spectra of the cocrystals were found to be relatable to the size of the HOCO-LUCO gap, which could be rationalised in terms of the frontier orbitals of Lawsone and the coformer. From our electronic-structure analyses, the H-bonding appears to raise and lower the energies of the Lawsone and coformer orbitals, respectively, ultimately leading to the energy gap in the adduct being 200-400 meV lower than those of the component species. The intermolecular interactions between heterodimers in the crystal lead to a further narrowing of the gap of a similar magnitude.

In summary, the combined experimental and theoretical approach taken in this study has allowed us to gain some interesting insight into the energetics and origin of the colour shift in cocrystals of the Lawsone molecule, which we hope will contribute to future crystal-engineering studies on this and related systems.

Methods

Lawsone (2-hydroxy-1,4-naphthoquinone), 4,4'-bipyridine, 4-(2-pyridine-4-ethyl)pyridine, 2-hydroxy pyridine and 1,3-di(4-pyridyl)propane were purchased from Sigma Aldrich and used without further processing. Cocrystals **1a**-**1c** were formed by dissolving Lawsone and the conformer in methanol in a 2:1 molar ratio and allowing them to crystallise. Cocrystal **1c** owing to higher solubility tended to crytallise only at low temperatures (typically below 4ºC) and tended to redissolve if left at room temperature for too long. **1d** was obtained by dissoving Lawsone and 2-hydroxy pyridine in dichloromethane in a 1:1 molar ratio, with toluene being added to the mixture to reduce the rate of evaporation.

UV-visible absorption spectra were recorded in a 2:1 mixture of acetonitrile and methanol to prevent the cocrystals from dissociating, and were measured using the Cary 60 Spectrophotometer (Agilent). Reflectance spectra were recorded at using a home built spectrometer on loan from Mobile Labs (CHARISMAA initiative) with a resolution of 8 nm. The instrument was not available at the time of preparation of **1d**, and thus we were not able to collect a spectrum of **1d**. Single-crystal diffraction data on **1a**-**1c** was obtained using an Oxford Xcaliber diffractometer with a Mo (Kα) source (wavelength 0.71073 Å) at 180 k. The structure was solved using SHELXL-97[24] .The diffraction pattern of **1d** was collected on a similar instrument at 150K, solved using SHELXT[25] and refined using the OSCAIL software. A comparison between the powder patterns obtained from the filtrate, and the simulated powder patter from the single crystal structure, show a good match suggesting that the adducts obtained via solution crystallisation have no residual starting materials (see supporting information).

Computational modelling was carried out within the Kohn-Sham density-functional theory framework,[26, 27] as implemented in the Vienna *Ab Initio* Simulation Package (VASP) code.[28]

Initial models of the crystal structures of **1a**-**1d** were built from the X-ray structures. In addition to these crystalline models, gas-phase models of Lawsone, coformers **a**-**d**, the $\mathbf{d}_2$ dimer and heterodimers **1a**-**1d** were created by extracting the atomic coordinates of each species/adduct from the crystal structures, and placing them in a simulation cell with an initial 10 Å vacuum gap between the closest atoms in adjacent periodic images.

Geometry optimisations and initial total-energy calculations were carried out with the PBEsol functional[20] with projector augmented-wave (PAW) pseudopotentials[29, 30] and a plane-wave kinetic-energy cutoff of 850 eV. In the calculations on the crystalline models, the Brillouin zone was sampled with Γ-centred Monkhorst-Pack ***k***-point meshes[31] with 1×3×1, 3×1×1, 1×1×3 and 1×3×1 subdivisions for **1a**, **1b**, **1c** and **1d**, respectively. This corresponds to two irreducible ***k***-points in each structure. In the gas-phase calculations, the electronic wavefunctions were evaluated at the Γ point. These convergence parameters were sufficient to converge the absolute total energies to within 1 meV $atom^{-1}$, and the pressure to well within 1 kbar (0.1 GPa). The electronic wavefunctions were optimised to a tolerance of 10^{-6} eV, and the positions of the ions, and also the cell shape/volume in the case of the crystalline models, were optimised until the magnitude of the forces on the ions was less than 10^{-2} eV $Å^{-1}$.

Electronic-structure calculations, including the evaluation of energy gaps, the orbital analyses, and the computation of absorption spectra, were performed using the PBE0 hybrid functional[21] using the PBEsol-optimised structures as input. The absorption spectra were computed using the linear-optics routines in VASP,[32] and the number of electronic bands was increased to 3× the default value in these calculations in order to ensure the convergence of the sum over empty states.

We note that, due to the size of the unit cell of the **1c** crystal (536 atoms), we had to reduce the plane-wave cutoff to 550 eV for the PBE0 calculations on this system. This is still above 1.3× the default cutoff recommended for the pseudopotentials we used, and so we expect it should give reasonable absorption spectra and charge/orbital densities; however, the total energies cannot be compared with those calculated using higher cutoffs, and so we did not include PBE0 formation energies for this compound in Table 1.

Acknowledgements

The authors are grateful to Dr. John E. Davies for collecting single-crystal X-ray data for the reported cocrystals. AP is grateful to Prof Stephen R. Elliott for hosting her for her doctoral studies. AP is also grateful to MOLABS, part of a European initiative called CHARISMAA, for lending their reflectance spectrometer. JMS gratefully acknowledges financial support from an EPSRC Programme Grant (no. EP/K004956/1). The computational modelling was carried out using the Balena HPC system, maintained by the Bath University Computing Service, and the ARCHER supercomputer, accessed through membership of the UK's HPC Materials Chemistry Consortium, which is funded by EPSRC Grant No. EP/L000202.

Data-Access Statement

The structures of the reported cocrystals **1a-1d** are available free of charge from the CCDC (codes **[X]**, **[Y]**, **[Z]** and **[W]**). The PBEsol-optimised gas-phase structures of **1**, coformers **a-d**, the $\mathbf{d}_2$ dimer, and heterodimers **1a-1d**, as well as the optimised crystal structures of **1a-1d**, are available online at **[TODO(!)]**. All other experimental characterisation and simulation results are presented in the manuscript and supporting information, with raw data available from the authors on request.

Notes and references

[a]Present address: School of Chemistry, National University of Ireland, Galway, Ireland

[b]*Present address*: Department of Pure and Applied Chemistry, University of Strathclyde, Thomas Graham Building, 295 Cathedral Street, Glasgow,United Kingdom, G1 1XL

[c]Present address: Department of Chemistry, University of Bath, Claverton Down, Bath, BA2 7AY, UK

[d]Department of Chemistry, University of Cambridge, Cambridge, CB2 1EW, UK

*To whom correspondence should be addressed. E-mail: *jms70@bath.ac.uk; Tel: +44 1223 336 468*

†Electronic Supplementary Information (ESI) available: [CCDC 851715-851717, Crystallographic Tables, Hydrogen bond tables, Computed spectra of cocrystals and response density figures]. See DOI: 10.1039/b000000x/

1. A. C. Dweck, *International journal of cosmetic science*, 2002, **24**.
2. N. M. Rahmoun, Z. Boucherit-Otmani, K. Boucherit, M. Benabdallah, D. Villemin and N. Choukchou-Braham, *Medecine Et Maladies Infectieuses*, 2012, **42**.
3. N. Sritrairat, N. Nukul, P. Inthasame, A. Sansuk, J. Prasirt, T. Leewatthanakorn, U. Piamsawad, A. Dejrudee, P. Panichayupakaranant, K. Pangsomboon, N. Chanowanna, J. Hintao, R. Teanpaisan, W. Chaethong, P. Yongstar, N. Pruphetkaew, V. Chongsuvivatwong and W. Nittayananta, *Journal of Oral Pathology & Medicine*, 2011, **40**.
4. A. Ostovari, S. M. Hoseinieh, M. Peikari, S. R. Shadizadeh and S. J. Hashemi, *Corrosion Science*, 2009, **51**, 1935-1949.
5. S. B. Zaware, R. G. Gonnade, D. Srinivas, A. Khan and S. Y. Rane, *New Journal of Chemistry*, 2011, **35**.
6. Y. Yasin, N. M. Ismail, M. Z. Hussein and N. Aminudin, *Journal of Biomedical Nanotechnology*, 2011, **7**.
7. R. Jelly, S. W. Lewis, C. Lennard, K. F. Lim and J. Almog, *Chemical Communications*, 2008.
8. A. P. Neves, M. D. Vargas, C. A. Tellez Soto, J. M. Ramos, L. d. C. Visentin, C. B. Pinheiro, A. S. Mangrich and E. I. P. de Rezende, *Spectrochimica Acta Part a-Molecular and Biomolecular Spectroscopy*, 2012, **94**.
9. C. E. Dalgliesh, *Journal of the American Chemical Society*, 1949, **71**.
10. F. Zsila and I. Fitos, *Organic & Biomolecular Chemistry*, 2010, **8**.
11. A. V. Todkary, R. Dalvi, S. S. Alunke-Gawali, J. Linares, F. Varret, J. Marrot, J. V. Yakhmi, M. Bhadbhade, D. Srinivas, S. P. Gejji and S. Y. Rane, *Spectrochimica Acta Part a-Molecular and Biomolecular Spectroscopy*, 2006, **63**.
12. S. Salunke-Gawali, L. Kathawate, Y. Shinde, V. G. Puranik and T. Weyhermueller, *Journal of Molecular Structure*, 2012, **1010**.
13. D.-K. Bucar, S. Filip, M. Arhangelskis, G. O. Lloyd and W. Jones, *Crystengcomm*, 2013, **15**, 6289-6291.
14. Dongpeng Yan, A. Delori, G. O. Lloyd, T. Friščić, G. M. Day, W. Jones, J. Lu, M. Wei, D. G. Evans and X. Duan, *Angew. Chem.* , 2011, **123**, 12691 –12694.
15. S. E. KRIKORIAN and M. MAHPOUR, *Spectrochimica Acta A* 1973, **29**, 1233 - 1246.
16. J. Seliger and V. Zagar, *Journal of Physical Chemistry A*, 2013, **117**, 1651-1658.
17. M. Telzhensky and M. Kaftory, *Acta Crystallographica Section C-Crystal Structure Communications*, 2009, **65**, O314-O320.
18. P. Vishweshwar, J. A. McMahon, J. A. Bis and M. J. Zaworotko, *Journal of Pharmaceutical Sciences*, 2006, **95**, 499-516.
19. L. R. MacGillivray, *Journal of Organic Chemistry*, 2008, **73**, 3311-3317.
20. J. P. Perdew, A. Ruzsinszky, G. I. Csonka, O. A. Vydrov, G. E. Scuseria, L. A. Constantin, X. L. Zhou and K. Burke, *Physical Review Letters*, 2008, **100**.
21. C. Adamo and V. Barone, *J. Chem. Phys.*, 1999, **110**, 6158-6170.
22. J. M. Skelton, E. Lora da Silva, R. Crespo-Otero, L. E. Hatcher, P. R. Raithby, S. C. Parker and A. Walsh, *Faraday Discussions*, 2015.
23. K. T. Butler, C. H. Hendon and A. Walsh, *Journal of the American Chemical Society*, 2014, **136**, 2703-2727-2706.
24. G. M. Sheldrick, *Acta Crystallogr. C*, 2015, **71**, 3-8.
25. G. M. Sheldrick, *Acta Crystallogr. A*, 2015, **71**, 3-8.
26. W. Kohn and L. J. Sham, *Physical Review*, 1965, **140**, 1133-1138.
27. P. Hohenberg and W. Kohn, *Physical Review B*, 1964, **136**, 864-871.
28. G. Kresse and J. Hafner, *Physical Review B*, 1993, **47**.
29. P. E. Blochl, *Physical Review B*, 1994, **50**, 17953-17979.
30. G. Kresse and D. Joubert, *Physical Review B*, 1999, **59**.
31. H. J. Monkhorst and J. D. Pack, *Physical Review B*, 1976, **13**, 5188-5192.
32. M. Gajdos, K. Hummer, G. Kresse, J. Furthmuller and F. Bechstedt, *Physical Review B*, 2006, **73**.

Graphical abstract